

# Analysis of Stops With Small Stop-Neutralino Mass Difference at a LC

C. Milsténe, M. Carena, A. Freitas

*Fermi National Accelerator Laboratory, Batavia, IL 60510-500, USA*

A. Finch, A. Sopczak

*Lancaster University, Lancaster LA1 4YB, United Kingdom*

H. Nowak

*Deutsches Elektronen-Synchrotron DESY, D-15738 Zeuthen, Germany*

A compelling framework to explain dark matter and electroweak baryogenesis is supersymmetry with light scalar top quarks (stops) and a small mass difference between the stop and the lightest neutralino. In this work, the stop detection capability at the ILC for small mass differences between the stop and the neutralino is studied. The analysis is based on a fast and realistic detector simulation. Significant sensitivity for mass differences down to 5 GeV is obtained. It is discussed how the relevant parameters of the scalar tops can be extracted and used to compute the dark matter density in the universe.

## 1. INTRODUCTION

The origin and stabilization of electroweak symmetry, the nature of dark matter and the generation of the baryon asymmetry (baryogenesis) in the universe suggest the existence of new symmetries within the reach of next generation colliders. A particular attractive extension of the Standard Model that addresses all these issues is supersymmetry with TeV-scale supersymmetry breaking.

A long history of experimental observations has corroborated the evidence for dark matter in the universe, culminating in the recent accurate determination by the WMAP satellite, in combination with the Sloan Digital Sky Survey (SDSS) [1],  $\Omega_{\text{CDM}} h^2 = 0.1126^{+0.0161}_{-0.0181}$  at the 95% C.L. Here  $\Omega_{\text{CDM}}$  is the dark matter energy density normalized to the critical density and  $h$  is the Hubble parameter in units of 100 km/s/Mpc. Supersymmetry with  $R$ -parity conservation provides a natural dark matter candidate, which in most scenarios is the lightest neutralino.

Electroweak baryogenesis is based on the concept that the baryon asymmetry is generated at the electroweak phase transition. While in the Standard Model the phase transition is not sufficiently strongly first order and there is not enough CP violation, supersymmetry can alleviate both shortcomings. A strong first-order phase transition can be induced by loop effects of light scalar top quarks (stops) to the finite temperature Higgs potential. In much of the parameter space of interest for electroweak baryogenesis, the light stop is only slightly heavier than the lightest neutralino, thus implying that stop-neutralino co-annihilation is significant. The co-annihilation contribution is important to meet the WMAP experimental results shown above. In the co-annihilation region, the stop-neutralino mass difference is smaller than 30 GeV [2], making a discovery of the stops at hadron colliders difficult [3].

This work investigates the capabilities of a future international  $e^+e^-$  linear collider (ILC) to discover light stops and measure their properties. This study extends the reach of an earlier work [4] to the region of small stop-neutralino mass differences. The experimental analysis for the ILC is used to assess possible conclusions about the nature of dark matter.

## 2. EXPERIMENTAL SIMULATION

In this work, the production of light stops at a 500 GeV linear collider is analyzed, using high luminosity  $\mathcal{L} \sim 500 \text{ fb}^{-1}$  and polarization of both beams. For small mass differences  $\Delta m = m_{\tilde{t}_1} - m_{\tilde{\chi}_1^0}$ , a light stop decays dominantly

Table I: Cross-sections for the stop signal and Standard Model background processes for  $\sqrt{s} = 500$  GeV and different polarization combinations. The signal is given for the stop mixing angle  $\cos \theta_{\tilde{t}} = 0.5$ . Negative/positive polarization values refer to left-/right-handed polarization, respectively.

| Process                     | Cross-section [pb]          |           |           |
|-----------------------------|-----------------------------|-----------|-----------|
| $P(e^-)/P(e^+)$             | 0/0                         | -80%/+60% | +80%/-60% |
| $\tilde{t}_1 \tilde{t}_1^*$ | $m_{\tilde{t}_1} = 120$ GeV | 0.115     | 0.153     |
|                             | $m_{\tilde{t}_1} = 140$ GeV | 0.093     | 0.124     |
|                             | $m_{\tilde{t}_1} = 180$ GeV | 0.049     | 0.065     |
|                             | $m_{\tilde{t}_1} = 220$ GeV | 0.015     | 0.021     |
| $W^+W^-$                    | 8.55                        | 24.54     | 0.77      |
| $ZZ$                        | 0.49                        | 1.02      | 0.44      |
| $W e \nu$                   | 6.14                        | 10.57     | 1.82      |
| $eeZ$                       | 7.51                        | 8.49      | 6.23      |
| $q\bar{q}, q \neq t$        | 13.14                       | 25.35     | 14.85     |
| $t\bar{t}$                  | 0.55                        | 1.13      | 0.50      |
| 2-photon, $p_t > 5$ GeV     | 936                         | 936       | 936       |

into a charm quark and the lightest neutralino,  $\tilde{t}_1 \rightarrow c \tilde{\chi}_1^0$ . The signature for stop pair production at an  $e^+e^-$  collider,

$$e^+e^- \rightarrow \tilde{t}_1 \tilde{t}_1^* \rightarrow c\bar{c} \tilde{\chi}_1^0 \tilde{\chi}_1^0, \quad (1)$$

is two charm jets plus missing energy. For small  $\Delta m$ , the jets are relatively soft and separation from backgrounds is very challenging. Backgrounds arising from various Standard Model processes can have cross-sections that are several orders of magnitude larger than the signal, so that even small jet energy smearing effects can be important. The possibility of efficient charm tagging plays an important role in the signal identification and depends on the vertex detector performance. Thus it is necessary to study this process with a realistic detector simulation. Signal and background events are generated with PYTHIA 6.129 [5] with CIRCE for realistic beamstrahlung [6], together with additional private code for the stop signal generation previously used in Ref. [4]. The detector simulation is based on the fast simulation SIMDET [7], describing a typical ILC detector.

Tab. I lists the cross-sections for the signal process and the relevant backgrounds. They have been computed with the Monte-Carlo code used in Ref. [8] and by GRACE 2.0 [9], with cross-checks to COMPHEP 4.4 [10] where applicable. A minimal transverse momentum cut,  $p_t > 5$  GeV, is applied for the two-photon background, to avoid the infrared divergence.

In the first step of the event selection, the following cuts are applied:

$$\begin{aligned} 4 < N_{\text{charged tracks}} < 50, \quad & p_t > 5 \text{ GeV}, \\ |\cos \theta_{\text{thrust}}| < 0.8, \quad & |p_{\text{long,tot}}/p_{\text{tot}}| < 0.9, \\ E_{\text{vis}} < 0.75\sqrt{s}, \quad & m_{\text{inv}} < 200 \text{ GeV}. \end{aligned} \quad (2)$$

The cut on the number of charged tracks removes most leptonic background and part of the  $t\bar{t}$  background. By requiring a minimal transverse momentum  $p_t$ , the two-photon background and back-to-back processes like  $q\bar{q}$  are largely reduced. The signal is characterized by large missing energy and transverse momentum from the two neutralinos, whereas for most backgrounds the missing momentum occurs from particles lost in the beam pipe. Therefore, cuts on the thrust angle  $\theta_{\text{thrust}}$ , the longitudinal momentum  $p_{\text{long,tot}}$ , the visible energy  $E_{\text{vis}}$  and the total invariant mass  $m_{\text{inv}}$  are effective on all backgrounds. As can be seen in Tab. II, the various background are substantially reduced after these preselection cuts, while roughly around 70% of the signal is preserved.

After generating large event samples with the preselection cuts for the various backgrounds as listed in Tab. II, the following final event selection cuts are applied to further improve the signal-to-background ratio:

1. Number of jets  $N_{\text{jets}} = 2$ . Jets are reconstructed with the Durham algorithm with the jet resolution parameter  $y_{\text{cut}} = 0.003 \times \sqrt{s}/E_{\text{vis}}$ . The cut reduces substantially the number of  $W$  and quark pair events.

Table II: Background event numbers and  $\tilde{t}_1\tilde{t}_1^*$  signal efficiencies in % (for various  $m_{\tilde{t}_1}$  and  $\Delta m$  in GeV) after preselection and each of the final selection cuts. In the last column the expected event number are scaled to a luminosity of  $500 \text{ fb}^{-1}$ . The cuts are explained in the text.

| Process                 | Total           | After presel. | Scaled to 500 $\text{fb}^{-1}$ |       |       |       |       |       |       |
|-------------------------|-----------------|---------------|--------------------------------|-------|-------|-------|-------|-------|-------|
|                         |                 |               | cut 1                          | cut 2 | cut 3 | cut 4 | cut 5 | cut 6 |       |
| $W^+W^-$                | 210,000         | 2814          | 827                            | 28    | 25    | 14    | 14    | 8     | 145   |
| $ZZ$                    | 30,000          | 2681          | 1987                           | 170   | 154   | 108   | 108   | 35    | 257   |
| $W\ell\nu$              | 210,000         | 53314         | 38616                          | 4548  | 3787  | 1763  | 1743  | 345   | 5044  |
| $eeZ$                   | 210,000         | 51            | 24                             | 20    | 11    | 6     | 3     | 2     | 36    |
| $q\bar{q}, q \neq t$    | 350,000         | 341           | 51                             | 32    | 19    | 13    | 10    | 8     | 160   |
| $t\bar{t}$              | 180,000         | 2163          | 72                             | 40    | 32    | 26    | 26    | 25    | 38    |
| 2-photon                | $8 \times 10^6$ | 4061          | 3125                           | 3096  | 533   | 402   | 0     | 0     | < 164 |
| $m_{\tilde{t}_1} = 140$ | $\Delta m = 20$ | 50,000        | 68.5                           | 48.8  | 42.1  | 33.4  | 27.9  | 27.3  | 20.9  |
|                         | $\Delta m = 40$ | 50,000        | 71.8                           | 47.0  | 40.2  | 30.3  | 24.5  | 24.4  | 10.1  |
|                         | $\Delta m = 80$ | 50,000        | 51.8                           | 34.0  | 23.6  | 20.1  | 16.4  | 16.4  | 10.4  |
| $m_{\tilde{t}_1} = 180$ | $\Delta m = 20$ | 25,000        | 68.0                           | 51.4  | 49.4  | 42.4  | 36.5  | 34.9  | 28.4  |
|                         | $\Delta m = 40$ | 25,000        | 72.7                           | 50.7  | 42.4  | 35.5  | 28.5  | 28.4  | 20.1  |
|                         | $\Delta m = 80$ | 25,000        | 63.3                           | 43.0  | 33.4  | 29.6  | 23.9  | 23.9  | 15.0  |
| $m_{\tilde{t}_1} = 220$ | $\Delta m = 20$ | 10,000        | 66.2                           | 53.5  | 53.5  | 48.5  | 42.8  | 39.9  | 34.6  |
|                         | $\Delta m = 40$ | 10,000        | 72.5                           | 55.3  | 47.0  | 42.9  | 34.3  | 34.2  | 24.2  |
|                         | $\Delta m = 80$ | 10,000        | 73.1                           | 51.6  | 42.7  | 37.9  | 30.3  | 30.3  | 18.8  |

2. Large missing energy,  $E_{\text{vis}} < 0.4\sqrt{s}$ . This is effective against  $W^+W^-$ ,  $ZZ$  and di-quark events. In addition, a window for the invariant jet mass around the  $W$ -boson mass,  $70 \text{ GeV} < m_{\text{jet,inv}} < 90 \text{ GeV}$ , is excluded to reduce the large  $W\ell\nu$  background.
3.  $q\bar{q}$  events are removed by requiring a minimal acollinearity angle  $\cos\phi_{\text{aco}} > -0.9$ .
4. Cutting on the thrust angle,  $|\cos\theta_{\text{thrust}} < 0.7|$ , reduces  $W$  boson background.
5. A strong cut on the transverse momentum,  $p_t > 12 \text{ GeV}$ , completely removes the remaining two-photon events.
6. The largest remaining background is from  $e^+e^- \rightarrow W\ell\nu$ . It resembles the signal closely in most distributions, *e.g.* as a function of the visible energy, thrust or acollinearity. Only by increasing the invariant jet mass window from cut 2 to ( $60 \text{ GeV} < m_{\text{jet,inv}} < 90 \text{ GeV}$ ), the signal-to-background ratio is improved, but at the cost of losing a substantial amount of the signal. In addition, the signal selection can be enhanced by charm tagging, which is implemented based on the neural network analysis described in Ref. [11]. The neural network has been optimized to reduce the  $W\ell\nu$  background while preserving the stop signal for small mass differences.

The resulting event numbers, scaled to a luminosity of  $500 \text{ fb}^{-1}$ , and the signal efficiencies are listed in Tab. II. After the final selection, the  $\tilde{t}_1\tilde{t}_1^*$  signal event numbers are of same order as the remaining background,  $N \sim \mathcal{O}(10^4)$ .

To explore the reach for very small mass differences  $\Delta m = m_{\tilde{t}_1} - m_{\tilde{\chi}_1^0}$ , signal event samples have been generated also for  $\Delta m = 10 \text{ GeV}$  and  $5 \text{ GeV}$ , see Tab. III. The signal efficiency drastically drops for  $\Delta m = 5 \text{ GeV}$ , as a result of the  $p_t$  cut (cut 5). An optimization of the event selection for very small  $\Delta m$  will be addressed in future work.

Based on the above results from the experimental simulations, the discovery reach of a 500 GeV  $e^+e^-$  collider can be estimated, see Fig. 1. To cover the whole parameter region, the signal efficiencies for the parameters points in Tab. III are interpolated. Then, the signal rates  $S$  are computed by multiplying the efficiency  $\epsilon$  obtained from the simulations with the production cross-section for each point  $(m_{\tilde{t}_1}, m_{\tilde{\chi}_1^0})$ . Together with the number of background events  $B$ , this yields the significance  $S/\sqrt{S+B}$ . The green area in the figure corresponds to the  $5\sigma$  discovery region,  $S/\sqrt{S+B} > 5$ . As evident from the figure, the ILC can find light stop quarks for mass differences down to  $\Delta m \sim \mathcal{O}(5 \text{ GeV})$ , covering the complete stop-neutralino co-annihilation region and beyond.

Table III: Signal efficiencies for  $t_1\bar{t}_1^*$  production after final event selection for different combinations of the stop mass  $m_{\tilde{t}_1}$  and mass difference  $\Delta m = m_{\tilde{t}_1} - m_{\tilde{\chi}_1^0}$ .

| $\Delta m$ | $m_{\tilde{t}_1} = 120$ GeV | 140 GeV | 180 GeV | 220 GeV |
|------------|-----------------------------|---------|---------|---------|
| 80 GeV     |                             | 10%     | 15%     | 19%     |
| 40 GeV     |                             | 10%     | 20%     | 24%     |
| 20 GeV     | 17%                         | 21%     | 28%     | 35%     |
| 10 GeV     | 19%                         | 20%     | 19%     | 35%     |
| 5 GeV      | 2.5%                        | 1.1%    | 0.3%    | 0.1%    |

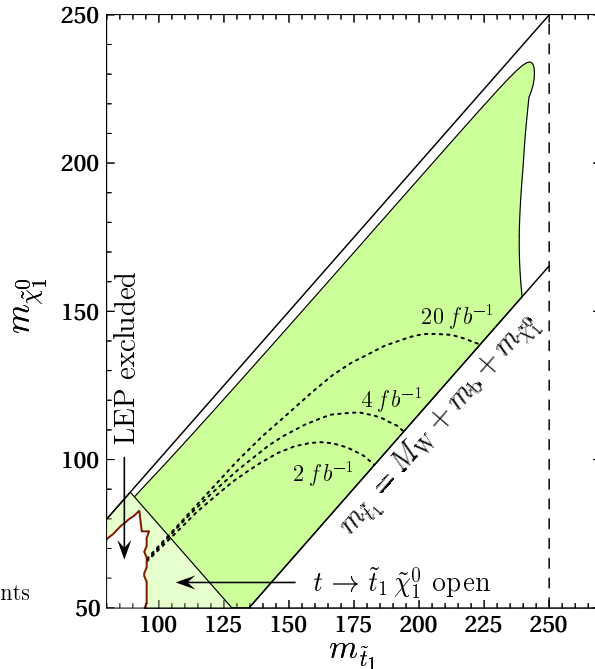


Figure 1: Discovery reach of linear collider with  $500 \text{ fb}^{-1}$  luminosity at  $\sqrt{s} = 500 \text{ GeV}$  for production of light stop quarks,  $e^+e^- \rightarrow \tilde{t}_1 \tilde{t}_1^* \rightarrow c\bar{c} \tilde{\chi}_1^0 \tilde{\chi}_1^0$ . The results are given in the stop vs. neutralino mass plane. In the dark shaded region, a  $5\sigma$  discovery is possible. The region where  $m_{\tilde{\chi}_1^0} > m_{\tilde{t}_1}$  is inconsistent with a neutralino LSP, while for  $m_{\tilde{t}_1} > M_W + m_b + \tilde{\chi}_1^0$  the three-body decay  $\tilde{t}_1 \rightarrow W^+ \bar{b} \tilde{\chi}_1^0$  becomes accessible and dominant. In the light shaded corner to the lower left, the decay of the top quark into a light stop and neutralino is open. Also shown are the parameter region excluded by LEP searches [12] (white area in the lower left) and the Tevatron light stop reach [3] (dotted lines) for various integrated luminosities.

### 3. STOP PARAMETER DETERMINATION

The discovery of light stops would hint towards the possibility of electroweak baryogenesis and may allow the co-annihilation mechanism to be effective. In order to confirm this idea, the relevant supersymmetry parameters need to be measured accurately. In this section, the experimental determination of the stop parameters will be discussed.

For definiteness, a specific MSSM parameter point is chosen:

$$\begin{aligned} m_{\tilde{U}_3}^2 &= -99^2 \text{ GeV}^2, & A_t &= -1050 \text{ GeV}, & M_1 &= 112.6 \text{ GeV}, & |\mu| &= 320 \text{ GeV}, \\ m_{\tilde{Q}_3} &= 4200 \text{ GeV}, & \tan \beta &= 5, & M_2 &= 225 \text{ GeV}, & \phi_\mu &= 0.2. \end{aligned} \quad (3)$$

The chosen parameters are compatible with the mechanism of electroweak baryogenesis, generating the baryon asymmetry through the phase of  $\mu$ . They correspond to a value for the dark matter relic abundance within the WMAP bounds,  $\Omega_{\text{CDM}}h^2 = 0.1122$ . The relic dark matter density has been computed with the code used in Ref. [13]. In this scenario, the stop and lightest neutralino masses are  $m_{\tilde{t}_1} = 122.5$  GeV and  $m_{\tilde{\chi}^0} = 107.2$  GeV, and

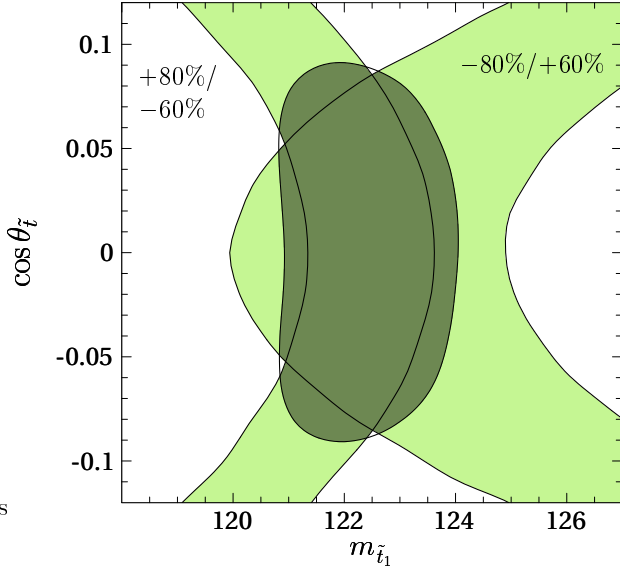


Figure 2: Determination of light stop mass  $m_{\tilde{t}_1}$  and stop mixing angle  $\theta_{\tilde{t}}$  from measurements of the cross-section  $\sigma(e^+e^- \rightarrow \tilde{t}_1\tilde{t}_1^*)$  for beam polarizations  $P(e^-)/P(e^+) = -80\%/+60\%$  and  $+80\%/-60\%$ . The plot includes statistical and systematic errors.

the stop mixing angle is  $\cos \theta_{\tilde{t}} = 0.0105$ , *i.e.* the light stop is almost completely right-chiral. The mass difference  $\Delta m = m_{\tilde{t}_1} - m_{\tilde{\chi}_1^0} = 15.2$  GeV lies within the sensitivity range of the ILC.

The measurement of  $\tilde{t}_1\tilde{t}_1^*$  production cross-section for different beam polarization allows to extract both the mass of the light stop and the stop mixing angle [14]. Here it is assumed that  $250 \text{ fb}^{-1}$  is spent each for  $P(e^-)/P(e^+) = -80\%/+60\%$  and  $+80\%/-60\%$ , where negative/positive polarization degrees indicate left-/right-handed polarization. Besides the statistical errors, the following systematic errors are taken into account: mass measurement of the lightest neutralino  $\delta m_{\tilde{\chi}_1^0} = 0.1$  GeV (see Ref. [15] for details); determination of the polarization degree  $\delta P(e^\pm)/P(e^\pm) = 0.5\%$ ; error in the integrated luminosity  $\delta \mathcal{L}/\mathcal{L} = 5 \times 10^{-4}$ ; theoretical uncertainty for background simulation  $\delta B/B = 0.3\%$ ; stop hadronization and fragmentation 0.5–1.0%; charm fragmentation and tagging efficiency  $\sim 0.5\%$ ; detector calibration  $\sim 0.5\%$ ; beamstrahlung uncertainty from [16].

Each of the two cross-section measurements for  $P(e^-)/P(e^+) = -80\%/+60\%$  and  $+80\%/-60\%$  correspond to a band in the parameter plane of the stop mass and mixing angle, see Fig. 2. Combining the two cross-section measurements, the stop parameter are determined to

$$m_{\tilde{t}_1} = (122.5 \pm 1.0) \text{ GeV}, \quad \cos \theta_{\tilde{t}} < 0.074 \quad \Rightarrow \sin \theta_{\tilde{t}} > 0.9972. \quad (4)$$

## 4. CONCLUSIONS

Using the data from the experimental stop analysis together with estimated errors for measurements in the neutralino/chargino sector, see Ref. [15], the expected cosmological dark matter relic density can be computed. The mass of the heavier stop  $\tilde{t}_2$  is too large to be measured directly, but it is assumed that a limit of  $m_{\tilde{t}_2} > 1000$  GeV can be set from collider searches.

All experimental errors are propagated and correlations are taken into account by means of a  $\chi^2$  analysis. The result of a scan over 100000 random points for the scenario eq. (3) is shown in Fig. 3. The horizontal bands depict the relic density as measured by WMAP [1], which is at  $1\sigma$  level  $0.104 < \Omega_{\text{CDM}}h^2 < 0.121$ . The collider measurements of the stop and chargino/neutralino parameters constrain the relic density to  $0.086 < \Omega_{\text{CDM}}h^2 < 0.143$  at the  $1\sigma$  level, with an overall precision of the same order of magnitude, though somewhat worse, than the direct WMAP determination. The uncertainty in the computation of the dark matter relic density from ILC precision measurements is dominated by the measurement of the lightest stop mass.

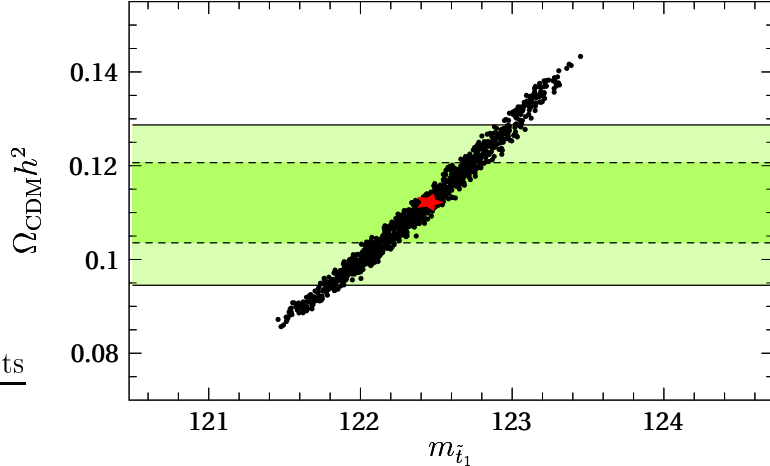


Figure 3: Computation of dark matter relic abundance  $\Omega_{\text{CDM}} h^2$  taking into account estimated experimental errors for stop, chargino, neutralino sector measurements at the ILC. The black dots correspond to a scan over the  $1\sigma$  ( $\Delta\chi^2 \leq 1$ ) region allowed by the experimental errors, as a function of the measured stop mass, with the red star indicating the best-fit point. The horizontal shaded bands show the  $1\sigma$  and  $2\sigma$  constraints on the relic density measured by WMAP.

## Acknowledgments

The authors are grateful to P. Bechtle, S. Mrenna and T. Kuhl for practical advice and to M. Schmitt for very useful discussions.

## References

- [1] D. N. Spergel *et al.* [WMAP Collaboration], *Astrophys. J. Suppl.* **148**, 175 (2003); M. Tegmark *et al.* [SDSS Collaboration], *Phys. Rev. D* **69**, 103501 (2004).
- [2] C. Balázs, M. Carena and C. E. M. Wagner, *Phys. Rev. D* **70**, 015007 (2004).
- [3] R. Demina, J. D. Lykken, K. T. Matchev and A. Nomerotski, *Phys. Rev. D* **62**, 035011 (2000).
- [4] A. Finch, H. Nowak and A. Sopczak, in *Prec. of the International Europhysics Conference on High-Energy Physics (HEP 2003), Aachen, Germany, 17-23 Jul 2003* [LC Note LC-PHSM-2003-075].
- [5] T. Sjöstrand *et al.*, *Comput. Phys. Commun.* **135**, 238 (2001).
- [6] T. Ohl, *Comput. Phys. Commun.* **101** (1997) 269.
- [7] M. Pohl and H. J. Schreiber, [hep-ex/0206009](#).
- [8] A. Freitas, D. J. Miller and P. M. Zerwas, *Eur. Phys. J. C* **21** (2001) 361; A. Freitas, A. von Manteuffel and P. M. Zerwas, *Eur. Phys. J. C* **34** (2004) 487.
- [9] F. Yuasa *et al.*, *Prog. Theor. Phys. Suppl.* **138**, 18 (2000).
- [10] E. Boos *et al.* [CompHEP Collaboration], *Nucl. Instrum. Meth. A* **534**, 250 (2004).
- [11] T. Kuhl, in *Proc. of the International Conference on Linear Colliders (LCWS 04), Paris, France, 19-24 Apr 2004*; T. Kuhl, LC Note in preparation.
- [12] LEP2 SUSY Working Group, ALEPH, DELPHI, L3 and OPAL experiments, note LEPSUSYWG/04-02.1.
- [13] C. Balázs, M. Carena, A. Menon, D. E. Morrissey and C. E. M. Wagner, *Phys. Rev. D* **71**, 075002 (2005).
- [14] A. Bartl, H. Eberl, S. Kraml, W. Majerotto, W. Porod and A. Sopczak, *Z. Phys. C* **76**, 549 (1997).
- [15] M. Carena, A. Finch, A. Freitas, C. Milsténe, H. Nowak, A. Sopczak, [hep-ph/0508152](#).
- [16] K. Mönig, in *Proc. of the 2nd ECFA/DESY LC Study (1998-2001)*, p. 1353-1361 [LC Note LC-PHSM-2000-060].